Journal of Electron Spectroscopy and Related Phenomena 183 (2011) 36–47

Contents lists available at ScienceDirect

Journal of Electron Spectroscopy and Related Phenomena

journal homepage: www.elsevier.com/locate/elspec

Interatomic electronic decay processes in singly and multiply ionized clusters

V. Averbukh[a,*], Ph.V. Demekhin[b], P. Kolorenč[c], S. Scheit[d], S.D. Stoychev[e], A.I. Kuleff[e], Y.-C. Chiang[e], K. Gokhberg[e], S. Kopelke[e], N. Sisourat[e], L.S. Cederbaum[e]

[a] Max Planck Institute for the Physics of Complex Systems, Nöthnitzer Str. 38, D-01187 Dresden, Germany
[b] Institut für Physik, Experimental-Physik IV, Universität Kassel, Heinrich-Plett-Str. 40, D-34132, Kassel, Germany
[c] Institute of Theoretical Physics, Faculty of Mathematics and Physics, Charles University in Prague, V Holešovičkách 2, 180 00 Prague, Czech Republic
[d] Department of Basic Science, Graduate School of Arts and Sciences, The University of Tokyo, 153-8902 Tokyo, Japan
[e] Theoretische Chemie, Physikalisch-Chemisches Institut, Universität Heidelberg, Im Neuenheimer Feld 229, D-69120 Heidelberg, Germany

ARTICLE INFO

Article history:
Available online 15 March 2010

Keywords:
Interatomic (intermolecular) decay
Decay cascade
Ab initio theory
Nuclear dynamics of electronic decay
Clusters

ABSTRACT

Since their theoretical prediction in 1997, interatomic (intermolecular) Coulombic decay (ICD) and related processes have been in the focus of intensive theoretical and experimental research. The spectacular progress in this direction has been stimulated both by the fundamental importance of the discovered electronic decay phenomena and by the exciting possibility of their practical application, for example in spectroscopy of interfaces. Interatomic decay phenomena take place in inner-shell-ionized clusters due to electronic correlation between two or more cluster constituents. These processes lead to the decay of inner-shell vacancies by electron emission and often also to disintegration of the resulting multiply ionized cluster. Here we review the recent progress in the study of interatomic decay phenomena in singly and multiply ionized clusters.

1. Introduction

The present day knowledge of interatomic (intermolecular) decay mechanisms in clusters encompasses a diversity of distinct physical phenomena, all stemming from interatomic (intermolecular) electronic interaction. In this section we give an overview of the predicted and observed interatomic decay processes induced by inner-shell ionization.

1.1. Interatomic (intermolecular) Coulombic decay

Core vacancy states of atoms and molecules represent very highly excited states of the corresponding atomic or molecular ions, typically lying above the double or even multiple ionization thresholds. As a result, these states decay by electron emission in a specific type of autoionization process named after its discoverer, Auger [1]. Kinetic energies of the electrons emitted in the course of Auger decay are given by the differences between the bound states of singly and doubly charged species and thus are quantized. This property explains the great spectroscopic value of the Auger electron spectroscopy (AES) [2], as well as its importance for numerous analytical applications, e.g. in surface science (see, for example, Ref. [3]). Auger decay is typically an intraatomic process, only modestly affected by the environment. Usually, such an effect is manifested in the so-called chemical shift of the Auger electron lines (see, for example, Ref. [4]).

In 1997, the authors of the theoretical work [5] took a pioneering approach to the issue of the environment effects on the decay of vacancy states [5]. The question posed by the authors was:

> Can a vacancy decay non-radiatively *only* due to the effect of the environment?

Surprisingly, it turned out that such an environment-mediated decay is not only possible, but is also a general phenomenon, typical of relatively low-energy inner-shell vacancies. In particular, clusters of various types prove to be the ideal objects to study this kind of decay phenomenon [5]. In order to get an idea of the new decay process discovered by Cederbaum and co-workers, one can consider the decay of 2*s* vacancy of neon, once in an isolated ion and once in a cluster, e.g. in Ne_n. The $2s^{-1}$ state of the isolated Ne^+ lies below the double ionization threshold of Ne and thus cannot decay by Auger mechanism. As a result, $(2s^{-1})$ Ne^+ decays radiatively on a nanosecond time scale. However, if $(2s^{-1})$ Ne^+ is allowed to interact with an environment, e.g. with other Ne atoms, the situation changes dramatically. Indeed, as shown schematically in Fig. 1 for neon dimer, in a Ne_n cluster, one can consider not only the high-energy $Ne^{2+}Ne_{n-1}$ doubly ionized states, but also the ones of the

* Corresponding author. Tel.: +49 351 871 1411; fax: +49 351 871 2299.
E-mail addresses: vitali@mpipks-dresden.mpg.de (V. Averbukh), philipp.demekhin@pci.uni-heidelberg.de (Ph.V. Demekhin), kolorenc@mbox.troja.mff.cuni.cz (P. Kolorenč), scheit@mns2.c.u-tokyo.ac.jp (S. Scheit), lorenz.cederbaum@pci.uni-heidelberg.de (L.S. Cederbaum).

0368-2048/$ – see front matter © 2010 Elsevier B.V. All rights reserved.
doi:10.1016/j.elspec.2010.03.003

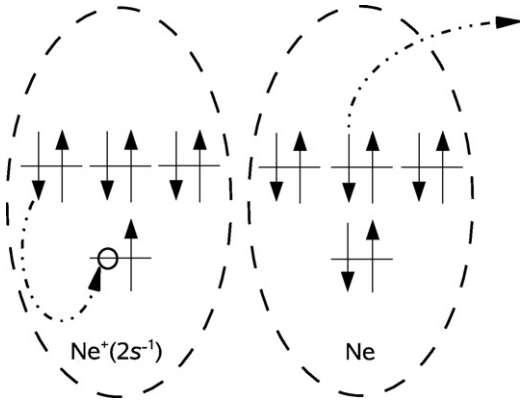

Fig. 1. A schematic representation of the ICD process in Ne dimer. 2*p* electron of the inner-valence-ionized Ne recombines into the 2*s* vacancy while a 2*p* electron of another Ne is ejected into continuum. The resulting doubly charged cluster decomposes by Coulomb explosion mechanism.

type $(Ne^+)_2Ne_{n-2}$. The latter states are relatively low in energy due to the separation of the positive charge between two neon atoms. In fact, the charge-separated states lie several electron-volts lower than $(2s^{-1})\ Ne^+Ne_{n-1}$. This leads to a very interesting *interatomic* decay process in which 2*p* electron of the ionized Ne fills the 2*s* vacancy, while 2*p* electron of another Ne atom is ejected into continuum. Since such a process is enabled by the Coulombic interaction between the electrons of the two Ne atoms, it has been called interatomic Coulombic decay (ICD). In a small loosely bound cluster, such as neon dimer, the repulsion between the two charges created by ICD leads to Coulomb explosion of the system [6] (see Ref. [7] for an exception). Under such conditions, the excess energy of the initial vacancy state is partitioned between the outgoing electron and the separating positively charged fragments. Thus, while Auger decay leads to quantized Auger electron energies, ICD in small clusters makes the total of the electron and the cluster fragment energies to be quantized. The kinetic energy of the relative motion of the fragments is often called kinetic energy release (KER).

The last several years have witnessed a series of remarkable advances in the experimental study of ICD. Hergenhahn, Möller and co-workers have presented the first experimental evidence of ICD by clearly identifying the new process in neon clusters [8]. Dörner, Jahnke and co-workers have conducted a detailed study of ICD in neon dimer [9] using the cold target recoil ion momentum spectroscopy (COLTRIMS) [10]. They have been able to measure in coincidence both the ICD electrons and the neon ions generated by the Coulomb explosion of $(Ne^+)_2$. The coincidences detected by Frankfurt group were found to be arranged along the energy conservation line corresponding to the sum of the electron energy and the KER being about 5 eV. Thus, the experiment of Dörner and co-workers constitutes the most detailed direct proof of the ICD. The electron kinetic energy and the KER spectra of Frankfurt group were later confirmed by theoretical calculations [11]. Going back to larger neon clusters, Örwall et al. have estimated the dependence of the ICD lifetime on the neon cluster size by distinguishing between the "bulk" and the "surface" peaks in the ICD electron spectra [12]. These experimental findings were found it to be in a reasonable agreement with earlier theoretical predictions of Santra et al. [13] (see also the more recent theoretical work of Vaval and Cederbaum [14]).

Both theoretical and experimental investigations have established ICD as a highly general and a very efficient decay process. Indeed, ICD is characteristic of vacancy states of van der Waals clusters (see, e.g. Refs. [5,8]), hydrogen bonded clusters (see, e.g. Refs. [16,15]), and even endohedral fullerenes [17]. The ICD lifetimes were found to belong to the range of 1–100 fs [13,12,17], many orders of magnitude shorter than those of the competing photon emission process. Thus, ICD is the main decay mode of moderate-energy (Auger-inactive) inner shell vacancies in clusters. Further studies of ICD are motivated, however, not only by the generality and efficiency of this new physical process, but also by the perspectives of its practical use, for example in spectroscopy. The very first step in this highly promising direction has been already done by Hergenhahn and co-workers who have shown that ICD electron spectra can be used in order to identify the Ne/Ar interface [18].

1.2. Beyond ICD of singly ionized states

1.2.1. Interatomic decay in inner-shell excitations

Recently, Barth et al. [19] have addressed the question, whether interatomic decay can occur not only in the inner-valence-ionized, but also in the inner-valence-excited states of clusters. They have created Ne $(2s^{-1}3p)$ excitations in Ne_n clusters (n being 70 on average) and detected the electrons emitted due to the $(2s^{-1}3p)NeNe_{n-1} \rightarrow (2p^{-1}3p)Ne(2p^{-1})Ne^+Ne_{n-2} + e^-$ process. Aoto et al. [20] studied in detail a similar decay phenomenon in neon dimer. This process is related to ICD exactly in the same way in which the resonant Auger effect [21,22] is related to the regular Auger effect [1,2]. Consequently, it has been called resonant interatomic Coulombic decay (RICD) [19].

RICD physics is richer and more involved that the ICD physics due to several reasons. First, the interatomic decay of inner-shell-excited states is accompanied by the intraatomic autoionization, e.g. $(2s^{-1}3p)Ne \rightarrow (2p^{-1})Ne + e^-$. Whereas ICD competes only with slow radiative decay, RICD has to compete with a fast non-radiative process. Nevertheless, both experimental [19,20] and theoretical [23] evidence show that this competition does not lead to a suppression of RICD. Another important difference between ICD and RICD comes from the fact that the inner-valence-excited electron can participate in RICD process. Exactly as the resonant Auger decay [21,22], RICD can occur either by *spectator* (*s*RICD) or by *participator* (*p* RICD) mechanism. While the *s* RICD process has been observed experimentally, *p*RICD has yet to be identified in the RICD electron spectra.

Yet another distinction between ICD and RICD has its origin in the higher energy accumulated in the inner-valence-excited states relative to the one of the inner-valence-ionized states. For example, $(2s^{-1}3p)Ne$ lies about 45.5 eV above the Ne ground state, whereas $(2s^{-1})\ Ne^+$ lies only about 26.9 eV above the Ne^+ ground state. As a result, decay of inner-valence-excited states can be accompanied by double ionization of the cluster. This can happen according to a variety of mechanisms which have been discussed qualitatively in Ref. [23]. The predicted double ionization interatomic processes still await their detailed quantitative study. The essential question is whether the double ionization processes are fast enough to compete with autoionization and *s* RICD. The subject of RICD will not be described in detail in this short review that will instead focus on the inter-atomic decay processes triggered by ionization.

1.2.2. Auger-ICD cascade

It is well known that Auger decay of core vacancies often results in highly excited states of the corresponding doubly ionized species. Sometimes, this brings about another stage (or even several stages) of Auger decay, forming what is usually called a decay cascade. Often, however, the excited doubly ionized states created by Auger process are not energetic enough to decay by an intraatomic mechanism. Under such conditions, formation of decay cascade is impossible in isolated species, but can occur in clusters with the second step of the cascade being of the ICD, rather than of the Auger type. The Auger-ICD cascade has been first predicted by Santra and Cederbaum [24] in 1*s*-ionized neon dimer and has

first been observed by Ueda and co-workers [25–27] in 2p-ionized argon dimers. Interestingly, the ICD process following the $2p^{-1} \rightarrow 3s^{-1}3p^{-1}$ Auger transition in argon dimer is energetically forbidden: the $3s^{-1}3p^{-1}$ states of Ar^{2+} are not energetic enough to lead to ICD [28]. Observation of Auger-ICD cascade in Ar_2 [25–27] has been nevertheless possible due to the fact that Auger decay populates not only the $3s^{-1}3p^{-1}$ main states, but also higher-energy satellites having admixture of $3p^{-3}3d$ configurations. The ICD following 2p ionization of the Ar dimers was theoretically interpreted in [28]. Later on, Auger-ICD cascade was also observed following 1s ionization of Ne dimer [29–31]. The ICD process was assigned as transition between the $(2s^{-1}2p^{-1}\,{}^1P)Ne^{2+}Ne$ and $(2p^{-2}\,{}^1D)Ne^{2+}$–$(2^{p-1})Ne^{+}$, and interpreted theoretically in [32]. More recently, relaxation pathways of the $Ne^{2+}Ar$ states populated via the K-LL Auger decay of $(1s^{-1})Ne^{+}Ar$ were analyzed in detail in [34]. Experimental work on the Auger-ICD cascade in NeAr is now in progress [35].

Further exploration of the fascinating subject of the interatomic decay phenomena and development of spectroscopic tools on their basis requires intensive theoretical effort to guide the experimental work. Such an effort is hardly possible without efficient, advanced theoretical tools involving both *ab initio* description of the electron correlation driving the decay and a treatment of the ensuing dynamics of the ionized cluster fragments. The next section gives the theoretical picture of interatomic decay within the Born–Oppenheimer (BO) approximation. *Ab initio* theory of interatomic decay widths is presented in some detail for the case of the ICD process in Section 3. Section 4 is devoted to the theory of Auger-ICD cascades. Some considerations on the future of the field are summarized in Section 5.

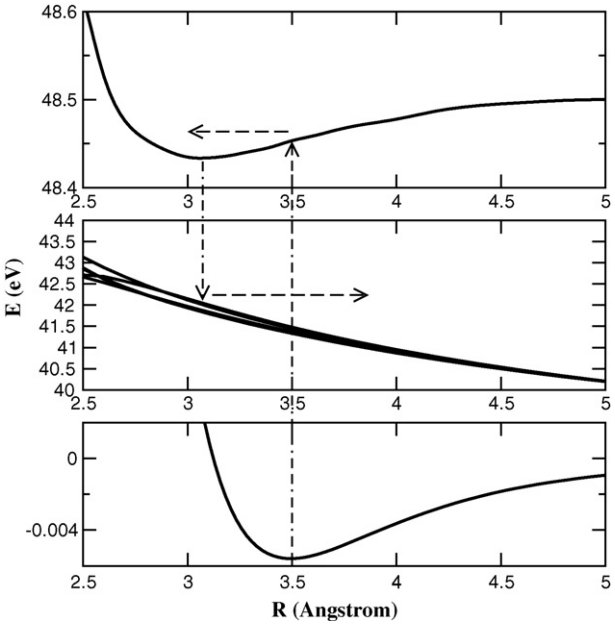

Fig. 2. Schematic representation of ICD process in Born–Oppenheimer picture. PESs of NeAr [38] are used as a representative example. Lower frame: ground state PES of the neutral diatom (initial state). Upper frame: inner-valence-ionized (intermediate state) PES. Middle frame: doubly ionized (final state) PESs. Transitions between the PESs accompanied by loss of an electron are shown by dashed-dotted lines. Directions of motion of nuclear wave packets on intermediate and final state PESs are shown by dashed lines.

2. Coupled electronic and nuclear dynamics of interatomic decay

The main objective of the theory of ICD is efficient and reliable calculation of the measurable spectra, i.e. ICD electron kinetic energy spectrum and (where applicable) KER spectrum. The theoretical description is usually given within Born–Oppenheimer approximation, in which the electronic states are decoupled from nuclear motion and depend only parametrically on the nuclear coordinates. In this picture, the inner shell ionization and the subsequent ICD process can be visualized as a series of transitions between potential energy surfaces (PESs) belonging to electronic states of different number of electrons (i.e. accompanied by electron emission). These transitions are represented schematically in Fig. 2. Initially, the system is assumed to be in the ground electronic state of the neutral (N-electron) system. The corresponding PESs of loosely bound clusters are characterized by shallow minima (e.g., in meV range for van der Waals systems) and large equilibrium interatomic distances. Photoionization brings the cluster almost instantaneously into inner-shell-ionized (typically, inner-valence-ionized) [$(N-1)$-electron] state, being the intermediate state of the decay. The PES of the singly ionized system is affected by the charge — induced dipole interaction that increases the binding energy and decreases the equilibrium interatomic distances relative to the van der Waals ground state. This means that after landing on the inner-shell-ionized PES, the nuclear wave packet is driven towards shorter internuclear distances. Due to the ICD, the intermediate state has finite lifetime. This means that the nuclear wave packet moving on the intermediate state PES can lose some of its density to the final (doubly ionized) state PESs. The latter are typically dominated by the repulsion between the two positive charges and are often close to the purely Coulombic repulsive shape. The geometry at which the decay occurred determines the partition of energy between the outgoing electron and the repelling fragments.

The above qualitative picture has its full formal analog in the so-called time-dependent formulation of the theory of nuclear dynamics of electronic decay processes. This theory is given in some detail in Ref. [11] and in references therein. Here we will consider only its few principal points. Let us denote the nuclear wave packets for the initial (i), intermediate (d) and final (f) electronic states as Ψ_i, Ψ_d, and Ψ_m^f, respectively, where the index m accounts for the possibility that there are several final electronic states (see Fig. 2). We assume that the electric field used in order to ionize the initial state is weak enough (weak-field approximation) and describe the coupling between the intermediate and the final states of the decay in the so-called local approximation [11]. Under these approximations, the nuclear wave packets obey the following set of coupled differential equations:

$$\begin{aligned} i\hbar\frac{\partial}{\partial t}|\Psi_i(R,t)\rangle &= \hat{H}_i(R)|\Psi_i(R,t)\rangle \\ i\hbar\frac{\partial}{\partial t}|\Psi_d(R,t)\rangle &= \hat{F}(R,t)|\Psi_i(R,t)\rangle + \hat{\mathcal{H}}_d(R)|\Psi_d(R,t)\rangle \\ i\hbar\frac{\partial}{\partial t}|\Psi_m^f(R,\epsilon,t)\rangle &= \hat{W}_m(R,\epsilon)|\Psi_d(R,t)\rangle + (\hat{H}_m^f(R)+\epsilon)|\Psi_m^f(R,\epsilon,t)\rangle, \end{aligned} \tag{1}$$

where ϵ is the energy of the electron emitted during ICD.

The Hamilton operators for the nuclear motion in the initial and final electronic states in (1) are defined as $\hat{H}_i = \hat{T}_N + \hat{V}_i$ and $\hat{H}_m^f = \hat{T}_N + \hat{V}_m^f$, where $\hat{T}_N$ is the nuclear kinetic energy and $\hat{V}_i$ and $\hat{V}_m^f$ are the initial and final state PESs, respectively. The effective Hamilton operator governing the intermediate state dynamics has to account for the fact that the intermediate state is an electronic resonance. Within the local approximation, this is done by lending the intermediate state Hamiltonian a non-Hermitian character:

$$\hat{\mathcal{H}}_d(R) = \hat{T}_N(R) + \hat{V}_d(R) - i\hat{\Gamma}(R)/2, \tag{2}$$

where $\hat{V}_d(R)$ is the intermediate state PES and $\hat{\Gamma}(R)$ is the total decay width.

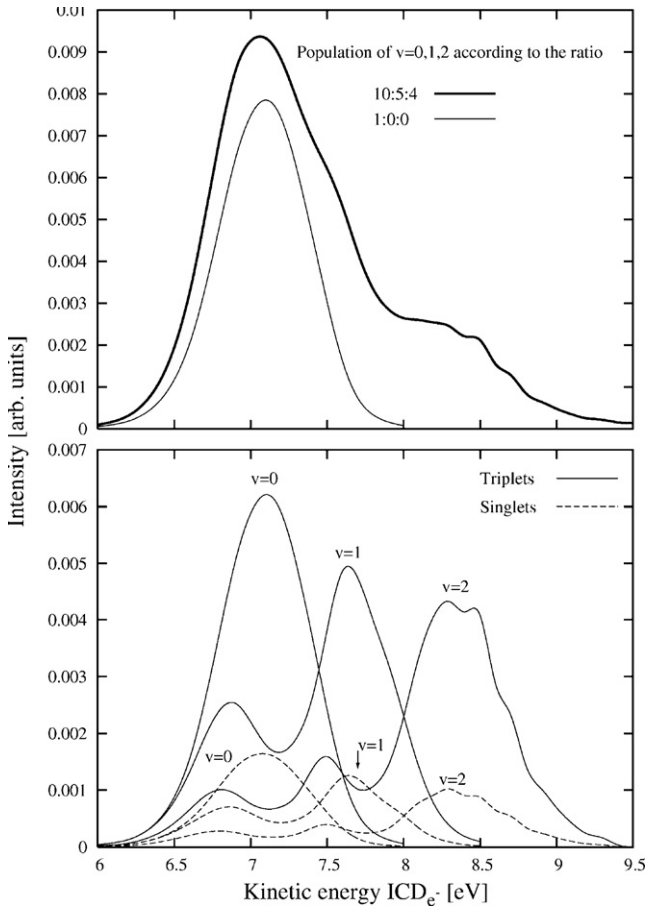

Fig. 3. ICD of 2*s* Ne vacancy in NeAr cluster. Lower panel: the singlet (dashed lines) and the triplet (solid lines) final state contributions to the ICD electron spectra for three different initial vibrational states of neutral NeAr: $v = 0, v = 1$, and $v = 2$. Upper panel: the total ICD electron spectra obtained assuming the population of the three lowest vibrational states of the electronic ground state to be according to the 10:5:4 ratio (solid line) and according to the 1:0:0 ratio (thin solid line). One can see that the ICD electron spectrum depends strongly on the initial vibrational state of the neutral cluster.

The coupling operators $\hat{F}$ and $\hat{W}_m$ describe the excitation from the initial to the intermediate electronic state and the coupling of the latter to the m-th final state, respectively. Since we assume the inner-shell ionization to occur instantaneously, $\hat{F}$ can be taken to be R-independent and simply a δ-function in time. The $\hat{W}_m$ operators describe the coupling of the intermediate state to the different final states. Within the local approximation, they are energy-independent and are related to the corresponding partial decay widths: $\Gamma_m(R) = 2\pi|\hat{W}_m(R)|^2$.

As shown, e.g., in Ref. [11,36,37], all the information concerning the decay spectrum can be derived from the knowledge of the final nuclear wave packets. Indeed, at sufficiently large time (i.e., when the decay is complete and the norm of all the intermediate wave packet is zero), only the final states are populated and thus carry all the spectroscopic information of interest. In particular, the decay spectrum as a function of the emitted electron energy ϵ is given by [11,36]:

$$\sigma(\epsilon) = \lim_{t\to\infty}\sum_m \sigma_m(\epsilon, t) = \lim_{t\to\infty}\sum_m \langle \Psi^f_m(R, \epsilon, t)|\Psi^f_m(R, \epsilon, t)\rangle. \qquad (3)$$

Examples of the ICD electron spectra calculated for a series of initial vibrational states of the neutral NeAr cluster [38] are given in Fig. 3.

Eqs. (1) show clearly that the shape of the spectrum (3) is determined by two competing time scales: that of the nuclear wave packet motion on the intermediate PES and that of the interatomic decay. If the decay is fast relative to the nuclear motion, the ICD occurs around the equilibrium geometry of the neutral (see Ref. [38] for a recent example of this kind). If, on the other hand, decay is slow on the scale of the nuclear wave packet evolution, ICD occurs within a wide range of geometries. In the latter case, various contributions are expected to interfere resulting in a complex pattern of $\sigma(E)$ [see Eq. (3)].

An alternative way to obtain the ICD electron spectrum is through the time-independent formulation. The time-independent theory uses the stationary vibrational eigenstates of the intermediate and final state PESs, $|n^d_k\rangle$ and $|n^{f_m}_j\rangle$, to express the ICD electron spectrum:

$$\sigma(\epsilon) = \sum_j \left| \sum_k \frac{(n^{f_m}_j|\hat{W}^*_m|n^d_k)(n^d_k|\hat{F}|n_0)}{\epsilon + E^{f_m}_j - E^d_n} \right|^2, \qquad (4)$$

(exclusive population of the vibrational ground state $|n_0\rangle$ of the initial state PES is assumed here). Eq. (4) can be derived using non-Hermitian quantum scattering theory (see, e.g., Ref. [39]). It closely resembles the well known Kramers–Heisenberg formula [40] used, for instance, for description of resonant X-ray emission (see Ref. [41] for an example of a physical situation where Kramers–Heisenberg-type expression is not applicable to the Auger/ICD electron spectrum). The important difference between Eq. (4) and the standard Kramers–Heisenberg formula stems from the fact that the $|n^d_k\rangle$ vibrational states in Eq. (4) are eigenstates of the *non-Hermitian* Hamilton operator $\hat{\mathcal{H}}_d$ (2) describing the intermediate resonant electronic state. As a result, one has to use the so-called c-product $(\cdot|\cdot)$ [see Eq. (4)] which is defined by $(f|g) = \langle f^*|g\rangle$ (see Ref. [42]). Clearly the time-independent and time-dependent formulations are absolutely equivalent [43], even though each of them gives a different insight in the spectrum. For instance, in the time-independent expression the role of the single vibrational states can be visualized. On the other hand, the time-dependent formalism allows to follow the time-evolution of the process and of the electron distribution, often simplifying the interpretation of the final spectrum. Clearly, an accurate computation of the ICD width, $\Gamma(R)$, of the intermediate electronic state is crucial for a reliable prediction of the ICD electron spectra within both time-dependent and time-independent approaches.

3. ICD widths by Fano-ADC method

Calculation of ICD widths can be achieved within one of the two main theoretical approaches. One of them relies on the introduction of complex absorbing potential (CAP) [44,45] into the $(N-1)$-electron Hamiltonian [46] (see Refs. [47] on the relation between the CAP method and the method of exterior complex scaling). The decay widths are then given by the imaginary parts of those eigenvalues of the resulting non-Hermitian Hamiltonian that are stationary with respect to the non-physical CAP parameters. The $(N-1)$-electron Hamiltonian can be represented using a variety of *ab initio* techniques, such as for example, configuration interaction (CI) or algebraic diagrammatic construction (ADC) [48]. The application of the CAP-CI method to calculation of ICD widths has been reviewed in detail in Ref. [49]. More recently, CAP-ADC method [49] based on the ADC representation of the many-electron Hamiltonian has been developed [50–52] and applied to ICD [14]. An alternative *ab initio* approach to calculation of the interatomic decay widths on which we would like to concentrate here [53] relies on Fano theory of resonances [54], ADC-ISR representation of the many-electron wave functions [55] and Stieltjes imaging technique [56].

3.1. ICD within Fano theory of resonances

Fano theory of resonances [54] as well as its generalized version [57,58] developed for the description of Auger decay widths represents the wave function Ψ_E at some energy E above threshold as a superposition of bound-like (Φ) and continuum-like (χ_ϵ) components, which can be thought of as the initial and final states of the decay:

$$\Psi_{\alpha,E} = a_\alpha(E)\Phi + \sum_{\beta=1}^{N_c} \int C_{\beta,\alpha}(E,\epsilon)\,\chi_{\beta,\epsilon}\,d\epsilon, \tag{5}$$

where the index β runs over the N_c possible decay channels. In the specific case of interatomic (intermolecular) decay in clusters, the bound part of the wave function, Φ, corresponds to the singly ionized state, typically created by the inner valence ionization of one of the cluster subunits. The state Φ is characterized by the mean energy:

$$E_\Phi = \langle\Phi|\hat{H}|\Phi\rangle, \tag{6}$$

H being the full Hamiltonian of the system. The N_c decay channels in Eq. (5) are defined by the doubly ionized states of the cluster characterized by the energies $E_\beta < E$, $\beta = 1,\ldots,N_c$, i.e. by the energetically accessible final states of the interatomic (intermolecular) decay. The continuum functions corresponding to the decay channels are assumed to diagonalize the Hamiltonian to a good approximation:

$$\langle\chi_{\beta',\epsilon'}|\hat{H}-E|\chi_{\beta,\epsilon}\rangle \approx (E_\beta+\epsilon-E)\,\delta_{\beta',\beta}\,\delta(E_{\beta'}+\epsilon'-E_\beta-\epsilon). \tag{7}$$

Using the assumption of uncoupled continuum functions, Fano theory provides an analytic expression for the evaluation of the decay width:

$$\Gamma = \sum_{\beta=1}^{N_c}\Gamma_\beta = 2\pi\sum_{\beta=1}^{N_c}\left|M_\beta(E_r,\epsilon_\beta)\right|^2,\ M_\beta(E,\epsilon) = \langle\Phi|\hat{H}-E|\chi_{\beta,\epsilon}\rangle, \tag{8}$$

where E_r is the real energy of the decaying state, $E_r \approx E_\Phi = \langle\Phi|\hat{H}|\Phi\rangle$ and ϵ_β is the asymptotic kinetic energy of the ejected electron for the decay channel β, $E_r = E_\beta + \epsilon_\beta$.

3.2. Initial and final states of the ICD by algebraic diagrammatic construction in the framework of the intermediate state representation

For the result (8) to be applicable to the computation of the interatomic decay rates, one has to provide sensible approximations for the multi-electron bound (Φ) and continuum ($\chi_{\beta,\epsilon}$) wave functions. In our case, these are wave functions of a singly ionized N-electron cluster, i.e. $(N-1)$-electron states. Such states can be conveniently constructed using the single ionization ADC technique. The ADC methodology has been originally developed within the Green's function formalism [48]. Here, however, we would like to briefly review the single ionization ADC from a different standpoint, using the intermediate state representation (ISR) as proposed by Schirmer [55].

Consider the Hartree–Fock (HF) ground state of the N-electron neutral cluster, Φ_0^N. One can form a complete orthonormal set of the $(N-1)$-electron basis functions, $\Phi_J^{(N-1)}$ applying the so-called physical excitation operators, $\{\hat{C}_J\}$, to the HF ground state:

$$\begin{aligned}&\Phi_J^{(N-1)} = \hat{C}_J\Phi_0^N\\ &\{\hat{C}_J\} \equiv \{c_i;\ c_a^\dagger c_i c_j,\ i<j;\ c_a^\dagger c_b^\dagger c_i c_j c_k,\ a<b,\ i<j<k;\ldots\},\end{aligned} \tag{9}$$

where c_i and $c_a^\dagger$ are annihilation and creation operators respectively, the subscripts $i,j,k,\ldots$ relate to the occupied spin-orbitals and the subscripts $a,b,c,\ldots$ relate to the unoccupied spin-orbitals. The basis set (9) is used in the familiar CI expansion of the wave function. This expansion, once truncated after some specific excitation class $[J]$, possesses such important drawbacks as slow convergence and lack of size-consistency. The ADC method overcomes these drawbacks by using a more complicated basis for the expansion of the $(N-1)$-electron wave functions. The idea is to apply the physical excitation operators, $\{\hat{C}_J\}$, to the perturbation-theoretically corrected, or "correlated" ground state of the neutral system,

$$\begin{aligned}&\Psi_J^0 = \hat{C}_J\Psi_0^N\\ &\Psi_0^N = \Phi_0^N + \Psi_0^{(1)} + \Psi_0^{(2)} + \Psi_0^{(3)} + \cdots,\end{aligned} \tag{10}$$

where $\Psi_0^{(n)}$ is the n th-order correction to the HF ground state obtained by the standard many-body perturbation theory (see, e.g. Ref. [59]). Unfortunately, the resulting correlated excited states (CES's), Ψ_J^0, are not orthonormal. ADC takes care of this problem by orthonormalizing them in two steps to obtain the so-called intermediate states, $\tilde{\Psi}_J$. First, Gram–Schmidt orthogonalization *between the excitation classes* is performed to obtain the "precursor" states, $\Psi_J^\#$:

$$\Psi_J^\# = \Psi_J^0 - \sum_{\substack{K\\ [K]<[J]}} \langle\tilde{\Psi}_K|\Psi_J^0\rangle\tilde{\Psi}_K, \tag{11}$$

i.e. the functions belonging to the higher [e.g. two-hole, one-particle (2h1p) or $[J]=2$] excitation class are made orthogonal to those of all the lower [in this case, only one-hole (1h) or $[K]=1$] excitation classes. Second, the precursor states are orthonormalized symmetrically *inside each excitation class*:

$$\tilde{\Psi}_J = \sum_{\substack{J'\\ [J']=[J]}} \left(\underline{\underline{\rho}}^{\#-(1/2)}\right)_{J',J}\tilde{\Psi}_{J'},\ \left(\underline{\underline{\rho}}^{\#}\right)_{J',J} = \langle\Psi_{J'}^\#|\Psi_J^\#\rangle, \tag{12}$$

where $\left(\underline{\underline{\rho}}^{\#}\right)_{J',J}$ is the overlap matrix of the precursor states belonging to the same excitation class. The above two-step procedure can be applied iteratively, noting that the correlated excited states of the lowest (1h) excitation class are by definition also the precursor states.

Any state of the $(N-1)$-electron system can be represented using the orthonormal basis of the intermediate states:

$$\Psi_q^{(N-1)} = \sum_i\sum_{[J]=i} Y_{q,J}\tilde{\Psi}_J. \tag{13}$$

The expansion coefficients, Y_J are obtained by the diagonalization of the Hamiltonian matrix constructed in the basis of the intermediate states. It is a crucial feature of the ADC approach that the Hamiltonian matrix elements of the type $\langle\tilde{\Psi}_J|\hat{H}|\tilde{\Psi}_J\rangle$ can be expressed analytically via the orbital energies and the electron repulsion integrals if one performs the orthonormalization procedure of Eqs. (11), (12) approximately and consistently with the order of the many-body perturbation theory which is used for the construction of the correlated ground state [see Eq. (10)]. Moreover, it can be shown [55] that truncation of the expansion (13) after the excitation class $[J]=m$ introduces an error of the order of $2m$, which should be compared to $m+1$ for the slower-converging CI expansion. The accuracy of the expansion in excitation classes (13) should be, of course, consistent with that of the perturbation theoretical series for the correlated ground state (10). Thus, the order, n, at which the perturbation theoretical expansion (10) is truncated is the single parameter defining the level of the ADC approximation. For this reason, ADC schemes of various quality are usually denoted

as ADC(n), $n = 2, 3, 4, \ldots$ in full analogy with the well-known MP2, MP3, MP4, ... perturbation-theoretical techniques for the ground state of the neutral system. The ADC(2) scheme for singly ionized states describes the many-electron wave-functions in the basis of 1h and 2h1p intermediate states treating the coupling between the 1h states and between 1h states and 2h1p states in the second and in the first order, respectively. ADC(2) approximation neglects the coupling between the different 2h1p basis functions. The extended ADC(2) scheme [ADC(2)x] takes into account the coupling between the 2h1p states in the first order (i.e. on CI level). The third-order ADC(3) scheme, while still confined to the basis of 1h and 2h1p intermediate states, treats the coupling between the 1h states and between 1h states and 2h1p states in the third and in the second order, respectively. A detailed description of the single ionization ADC(2) and ADC(3) schemes, including the expressions for the Hamiltonian matrix elements can be found in Ref. [60]. The proof of the size-consistency of the ADC(n) schemes has been given in Refs. [55]. The main limitation of the existing ADC(n) schemes is that they are applicable to ionized and/or excited states of closed-shell systems only. Here we are interested in applying ADC to the interatomic (intermolecular) decay in ionized van der Waals and hydrogen bonded clusters, all of which satisfy this requirement.

Our main purpose is to demonstrate that the ADC(n) schemes can be used for the *ab initio* calculations of the decay rates within Fano formalism. To this end, we need to show that both bound (Φ) and continuum ($\chi_{\beta,\epsilon}$) components of the $(N-1)$-electron wave function describing the decay process [see Eq. (5)] can be approximated by the expansion in the basis of the intermediate states (13). Suppose, a vacancy residing on the subunit A of a weakly bound cluster can decay by one of the interatomic (intermolecular) mechanisms, but cannot decay non-radiatively if created in the isolated species A. Clearly, in the final state of such a decay will be characterized by two vacancies, one or both of them residing on another cluster subunit. Thus, in order to construct the ADC(n) approximation for the bound part, Φ, one can restrict the physical excitation operators of the higher excitation classes to such where all the holes reside on the subunit A only:

$$\begin{aligned}&\Psi_J^0 = \hat{C}_J \Psi_0^N \\ &\{\hat{C}_J\} \equiv \{c_i;\ c_a^\dagger c_i c_j,\ i<j,\ \varphi_{i,j}\in A;\ c_a^\dagger c_b^\dagger c_i c_j c_k, \\ &a<b,\ i<j<k,\ \varphi_{i,j,k}\in A;\ldots\},\end{aligned} \tag{14}$$

where $\varphi_i \in A$ is an occupied spin-orbital of the neutral cluster localized on the subunit A. In this way, the intraatomic (intramolecular) relaxation and correlation effects inside the subunit A are taken into account, whereas any kind of interatomic decay cannot be described due to the restriction imposed on the holes. Upon the completion of the selection process, one can construct and diagonalize the Hamiltonian in the basis of the restricted set of the intermediate states using the standard methods. The ADC(n) state approximating the Φ component can be identified, for example, as the one possessing the maximal overlap with the cluster orbital representing the initial vacancy. Since no configurations corresponding to the open decay channels were used in the ADC-ISR expansion for the bound-like component, Φ, will be one of the lowest-energy eigenvectors of the ADC Hamiltonian. Therefore, a highly efficient Davidson diagonalization technique [61] can be used to diagonalize the matrix.

Once the ADC(n) approximation for the bound component of the wave function has been provided, the remaining task is to construct the approximate continuum components, $\chi_{\beta,\epsilon}$, describing the possible final states of the interatomic (intermolecular) decay. Such states are naturally found among the ADC(n) eigenstates of the 2h1p character:

$$\chi_{\beta,\epsilon} \sim \Psi_q^{2h1p} = \sum_i \sum_{[J]=i} Y_{q,J}\tilde{\Psi}_J,\ 1 - \sum_{[J]=2} |Y_{q,J}|^2 \ll 1. \tag{15}$$

The Ψ_q^{2h1p} functions can be constructed without any restriction of the kind of (14) being imposed on the physical excitation operators. It is, thus, possible that some intermediate states contribute both to Φ and to Ψ_q^{2h1p} expansions, leading to $\langle\Phi|\Psi_q^{2h1p}\rangle \neq 0$. This does not lead to complications as the Fano formalism that we are using does not assume the orthogonality of the bound and the continuum components. Application of the selection scheme described above is not straightforward in the case of symmetric clusters, e.g. those in which the ionized inner-shell orbital is delocalized due to inversion symmetry. As has been shown in Ref. [62], this difficulty can be circumvented by using the appropriate linear combinations of the "standard" configurations.

Despite the ability of ADC(n) to produce 2h1p-like wave functions in the continuum region of the spectrum, there still exists a major difficulty in associating these ADC(n) eigenstates with the approximate continuum states of Fano theory. The difficulty stems from the fact that the ADC(n) calculations, and *ab initio* quantum chemical calculations in general, are routinely performed using the $\mathcal{L}^2$ bases, usually the Gaussian ones. As a result, the $\mathcal{L}^2$ and not the scattering boundary conditions are imposed and the Ψ_q^{2h1p} functions are not properly normalized,

$$\langle\Psi_q^{2h1p}|\Psi_{q'}^{2h1p}\rangle = \delta_{q,q'} \tag{16}$$

[compare to Eq. (7)]. Moreover, the corresponding eigenenergies, E_q^{2h1p} are discrete and are not expected to fulfill the energy conservation relation for the non-radiative decay, $E_q^{2h1p} = E_\Phi$, except by a coincidence. An efficient way to deal with the above complications is provided by the computational approach known as Stieltjes–Chebyshev moment theory or Stieltjes imaging [56]. This approach rests on the fact that while decay width (8) cannot be calculated using the discretized continuum functions directly, the spectral moments of (8) calculated using the pseudospectrum are good approximations to the spectral moments constructed using the true continuum [56]:

$$\begin{aligned}&\sum_\beta \int E^k \left|\langle\Phi|\hat{H} - E_r|\chi_{\beta,\epsilon_\beta}\rangle\right|^2 dE \\ &\approx \sum_q \left(E_q^{2h1p}\right)^k \left|\langle\Phi|\hat{H} - E_r|\Psi_q^{2h1p}\rangle\right|^2.\end{aligned} \tag{17}$$

Using the techniques of moment theory, one can recover the correct value of the decay width (8) from the pseudospectrum through a series of consecutive approximations of increasing order, n_S [56]. A particularly efficient realization of the Stieltjes imaging procedure that we use in our work has been described in detail in Ref. [63].

3.3. Selected applications of the Fano-ADC method to interatomic decay widths in clusters

Interatomic decay widths as functions of cluster geometry are not only an essential input for simulations of ICD electron spectra [11,38], but are also very interesting physical quantities in their own right. The magnitude and the functional form of $\Gamma(R)$ can tell us a lot about physics of interatomic decay. For instance, at large distances, the ICD width can be shown to follow an inverse-power law, in most cases $\Gamma_{ICD}(R) \propto R^{-6}$ [13,49,16], see also [64]. This asymptotic behavior of the decay width can be explained by a physically appealing virtual photon transfer model which represents the decay process as an emission of a virtual photon by the inner-shell-

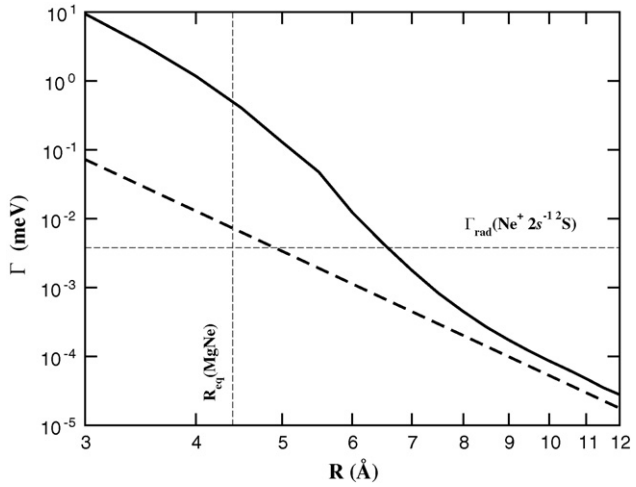

Fig. 4. Doubly logarithmic plot of the total ICD width of Ne 2*s* vacancy in MgNe cluster as a function of internuclear separation. Full line – ADC(2)x result, dashed line – virtual photon transfer prediction [16]. Radiative width of the 2*s* vacancy in free neon atom [66] and the equilibrium distance of MgNe in the ground state are shown by horizontal and vertical dashed lines, respectively.

ionized atom followed by its absorption by a neighboring neutral. The virtual photon transfer model neglects the overlap between the atomic orbitals of the atoms participating in the interatomic process and thus its validity around the equilibrium geometry of the neutral cluster was a subject of debate (see, e.g. Ref. [65]). Using the Fano-ADC *ab initio* approach of Sections 3.1 and 3.2, we have been able to show that the orbital overlap effect leads to a dramatic enhancement of ICD widths in rare gas–alkaline earth diatoms [16,53] (see Fig. 4). In rare gas clusters, such as Ne_2, the overlap enhancement of the ICD widths has a moderate character (see Fig. 5).

The discovery of the overlap effect on the ICD rates led us to ask the question of what kind of chemical environment leads to highest possible ICD rates retaining the clear-cut interatomic nature of the process. It has been realized quite early [13] that higher ICD rates are favored by environments with the highest possible number of nearest neighbors. In large neon clusters, for example, a "bulk" 2*s* vacancy would decay faster than the "surface" one [12]. It turns out, though, that even the "bulk" neon ICD rates can be outmatched by interatomic decay in a very interesting group of chemical compounds called endohedral fullerene complexes, e.g. in Ne@C_{60}[17]. Indeed, in $(2s^{-1})$ Ne^+@C_{60}, the inner valence ionized Ne has as many as 60 nearest neighbors to interact with, which leads to as many as several hundreds of ICD channels. As a result, the lifetime of $(2s^{-1})$ Ne^+@C_{60} is only about 2 fs, in fact shorter than Auger lifetime of isolated 1*s*-ionized neon atom [17]. The ultrafast character of ICD is not the only unique feature of interatomic decay in endohedral fullerenes. A detailed consideration of the possible decay pathways reveals that the relatively low multiple ionization energies of the fullerenes give rise to a number of intriguing new processes, such as double ICD (DICD) (being interatomic analog of double Auger decay [68]), double electron transfer mediated decay (DETMD) and a two-step cascade of interatomic decay [17]. A combination of ultrafast ICD with the rich pattern of the possible electronic decay channels makes endohedral fullerenes particularly attractive for future theoretical and experimental studies.

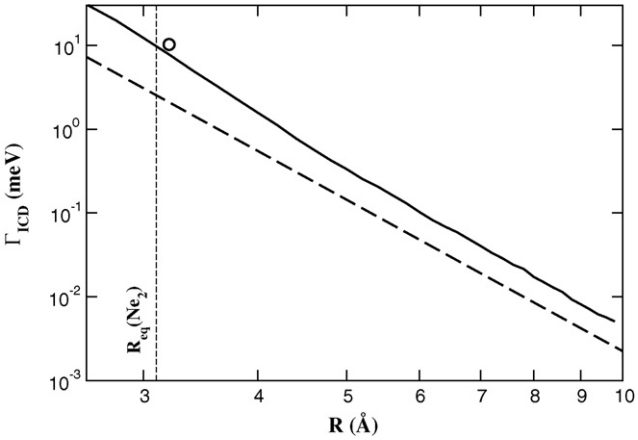

Fig. 5. Doubly logarithmic plot of the total ICD decay width of Ne 2*s* vacancy in Ne_2 cluster as a function of internuclear separation. Full line – ADC(2)x result, dashed line – virtual photon transfer prediction [62], full circle – the result of the single point multi-reference CAP-CI calculation of Ref. [67]. Equilibrium distance of Ne_2 in the ground state is shown by the vertical dashed line.

4. Interatomic decay in doubly ionized systems

As pointed out in Section 1.2.2, Auger decay of core vacancies often produces highly excited states of the corresponding doubly ionized species which can, in full analogy with the case of single inner-valence vacancy, undergo interatomic (intermolecular) decay of the ICD type in clusters. The last few years have witnessed a significant progress in the experimental investigation of ICD following Auger decay [25,29–31,27]. On the theoretical side, the success of the Fano-ADC method, described in Section 3, motivated extension of this approach to the description of the interatomic decay of excited doubly ionized states in clusters [69]. Moreover, the time-dependent nuclear dynamics theory of electronic decay has been generalized to the case of decay cascades [70,32,34].

4.1. Dynamics of Auger-ICD cascades

Let us consider Auger-ICD cascade in neon dimer as an example [32]. The relevant PESs of the Ne_2 computed in [33] are depicted in Fig. 6. The whole decay cascade can be described as the following step-wise process:

$$\begin{aligned} &Ne_2 + \hbar\omega_{exc} \rightarrow Ne_2^+(1s^{-1}) + e^-_{ph} \rightarrow \\ &Ne^{2+}(2s^{-1}2p^{-1}\,^1P)Ne + e^-_{ph} + e^-_{Aug} \rightarrow \\ &Ne^{2+}(2p^{-2}\,^1D) + Ne^+(2p^{-1}) + e^-_{ph} + e^-_{Aug} + e^-_{ICD}, \end{aligned} \tag{18}$$

Broadband synchrotron radiation with an energy slightly above the K-shell ionization threshold populates the $(1s^{-1})$ Ne_2^+ ionic states with emission of the primary photoelectron (e^-_{ph}). In the next step, the intra-atomic $K - L_1L_{2,3}(^1P)$ Auger decay of the $(1s^{-1})$ Ne_2^+ core-ionized states populates the one-site dicationic states $(2s^{-1}2p^{-1}\,^1P)$ Ne^{2+}Ne with emission of an Auger electron (e^-_{Aug}). The Auger decay lifetime of 2.5 fs is by two orders of magnitude shorter than the typical time scale of the vibrational motion in the core-ionized states $(1s^{-1})$ Ne_2^+ (300 fs [32]), thus practically excluding possible effect of the nuclear dynamics at the first step of the cascade. Thus, one can assume a vertical (instantaneous) transfer of the nuclear wave packet to the PESs of the final Auger states (see Fig. 6).

After its creation close to the right turning point of the PES of the $(2s^{-1}2p^{-1}\,^1P)$ Ne^{2+}Ne state, the intermediate wave packet starts to propagate in the direction of smaller internuclear distances and simultaneously to decay via ICD transition into the $(2p^{-2}\,^1D, 2p^{-1})Ne^{2+}$–$Ne^+$ tricationic states with emission of the ICD electron (see Fig. 6). The potential energy curves for the $(2p^{-2}\,^1D, 2p^{-1})$ Ne^{2+}–Ne^+ tricationic states exhibit a typical repulsive character with asymptotic behavior $\sim 2/R$ a.u. and cross the $(2s^{-1}2p^{-1}\,^1P)$ Ne^{2+}Ne dicationic states between 2.6 and 2.7 Å. Note, only the uppermost and the lowermost lying repulsive PESs are

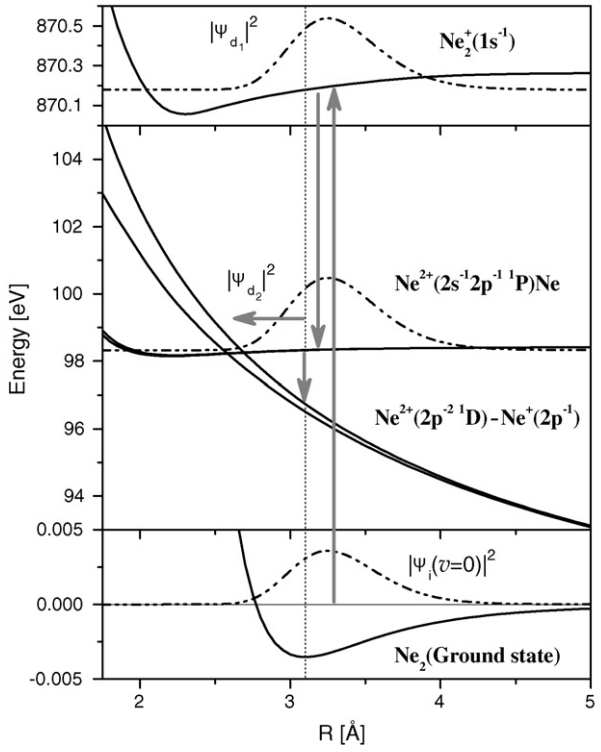

Fig. 6. PESs [33] of selected states of Ne_2 involved in the Auger-ICD cascade starting from the core ionization of the Ne dimer and consisting of one-site $K-L_1L_{2,3}(^1P)$ Auger transition in the Ne atom followed by ICD transition into the $(2p^{-2}\,{}^1D, 2p^{-1})Ne^{2+}$–$Ne^+$ states. The modulus square of the initial wave packet (dash-dot-dot line) centered around the equilibrium distance $R_e = 3.1$ Åof the initial state (indicated by a vertical dotted line) is also shown.

depicted in Fig. 6. The typical timescale of the vibrational motion in the $(2s^{-1}2p^{-1}\,{}^1P)$ $Ne^{2+}Ne$ states is about 300 fs [32] and is comparable with the lifetime for the electronic decay via ICD (100 fs [24]). As shown in [32], the competition between electronic decay and nuclear dynamics in this case influences the computed ICD spectra considerably (see Section 4.4).

The nuclear dynamics accompanying cascade decay (18) can be described in terms of the nuclear wave packets, propagating on the PESs of the initial, intermediate and final states, $|\Psi_i(R,t)\rangle$, $|\Psi_{d_1}(R,t)\rangle$, $|\Psi_{d_2}(R,\epsilon_1,t)\rangle$, and $|\Psi_f(R,\epsilon_1,\epsilon_2,t)\rangle$, respectively, satisfying the following system of coupled differential equations [32,70,34]:

$$\begin{aligned}
i\hbar\frac{\partial}{\partial t}|\Psi_i(R,t)\rangle &= \hat{H}_i(R)|\Psi_i(R,t)\rangle \\
i\hbar\frac{\partial}{\partial t}|\Psi_{d_1}(R,t)\rangle &= \hat{F}(R,t)|\Psi_i(R,t)\rangle + \hat{\mathcal{H}}_{d_1}(R)|\Psi_{d_1}(R,t)\rangle \\
i\hbar\frac{\partial}{\partial t}|\Psi_{d_2}(R,\epsilon_1,t)\rangle &= \hat{W}_1(R,\epsilon_1)|\Psi_{d_1}(R,t)\rangle \\
&\quad + \left(\hat{\mathcal{H}}_{d_2}(R)+\epsilon_1\right)|\Psi_{d_2}(R,\epsilon_1,t)\rangle \\
i\hbar\frac{\partial}{\partial t}|\Psi_f(R,\epsilon_1,\epsilon_2,t)\rangle &= \hat{W}_2(R,\epsilon_2)|\Psi_{d_2}(R,\epsilon_1,t)\rangle \\
&\quad + \left(\hat{H}_f(R)+\epsilon_1+\epsilon_2\right)|\Psi_m^f(R,\epsilon_1,\epsilon_2,t)\rangle,
\end{aligned} \tag{19}$$

where ϵ_1 and ϵ_2 are the energies of the Auger and ICD electrons, respectively; $\hat{\mathcal{H}}_{d_1}$ and $\hat{\mathcal{H}}_{d_2}$ are the nuclear effective Hamilton operators for the unstable intermediate states D_1 and D_2, respectively, given in the local approximation by expressions like Eq. (2); $\hat{H}_f$ is the nuclear Hamilton operator for the final state F; $\hat{F}(R,t)$, $\hat{W}_1(R,\epsilon_1)$, and $\hat{W}_2(R,\epsilon_2)$ are the transition operators between initial state I and intermediate state D_1, between intermediate states D_1 and D_2, and between intermediate state D_2 and final state F, respectively.

The nuclear wave packet $|\Psi_f(R,\epsilon_1,\epsilon_2,t)\rangle$ on the final state F contains all the necessary information on the spectra of the Auger and ICD electrons. The time evolutions of both spectra, $\sigma_{\mathrm{Aug}}(\epsilon_1,t)$ and $\sigma_{\mathrm{ICD}}(\epsilon_2,t)$, and the spectra, $\sigma_{\mathrm{Aug}}(\epsilon_1)$ and $\sigma_{\mathrm{ICD}}(\epsilon_2)$ themselves, can be computed as follows [32,70,34]:

$$\begin{aligned}
\sigma_{\mathrm{Aug}}(\epsilon_1,t) &= \int d\epsilon_2 ||\Psi_f(R,\epsilon_1,\epsilon_2,t)||^2, \quad \sigma_{\mathrm{Aug}}(\epsilon_1) = \lim_{t\to\infty}\sigma_{\mathrm{Aug}}(\epsilon_1,t), \\
\sigma_{\mathrm{ICD}}(\epsilon_2,t) &= \int d\epsilon_1 ||\Psi_f(R,\epsilon_1,\epsilon_2,t)||^2, \quad \sigma_{\mathrm{ICD}}(\epsilon_2) = \lim_{t\to\infty}\sigma_{\mathrm{ICD}}(\epsilon_2,t).
\end{aligned} \tag{20}$$

Eqs. (19) and (20) suggest that the Auger and ICD spectra can be strongly influenced by the interplay between time duration of the exciting pulse, lifetimes for the Auger and ICD transitions, and time scales for the nuclear dynamics on each decay step.

4.2. Fano-ADC method for interatomic decay widths in $(N-2)$-electron systems

Most computational aspects of the method are fully analogous to the single vacancy case and will not be repeated here. Instead, we will focus only on the few different points. Obviously, the principal difference is that the wave function Ψ_E of Eq. (5) represents now doubly ionized ($N-2$-electron) cluster. Therefore, double ionization ADC technique has to be used to construct the bound (Φ) and continuum ($\chi_{\beta,\varepsilon}$) $(N-2)$-electron states. Suitable ADC scheme for the *pp*-propagator has been derived by Schirmer and Barth [71]. To describe the bound component (Φ, initial state of the decay) of the wave function Ψ_E within the ADC(n) approach, it is necessary to restrict the physical excitation operators generating the CESs Ψ_J^0 (and, in turn, the intermediate states $\tilde{\Psi}_J$) in such a way that open channels of the interatomic decay are not included in the resulting basis.

The intraatomic nature of the Auger decay makes it possible to follow similar strategy as in Section 3.2, based on the spatial localization properties of the occupied spin-orbitals. Indeed, the initial state of the decay is characterized by two vacancies being localized on a single cluster constituent A, while in the triply ionized final states of Auger-ICD cascade, one or more vacancies reside on another cluster subunit. Therefore, in analogy with Eq. (14) the CESs for the initial state expansion are generated with the restriction that all the holes reside on the subunit A only:

$$\begin{aligned}
&\Psi_J^0 = \hat{C}_J\Psi_0^N \\
&\{\hat{C}_J\} \equiv \{c_ic_j, i<j, \varphi_{i,j}\in A;\ c_a^\dagger c_ic_jc_k, i<j<k, \varphi_{i,j,k}\in A;\ldots\},
\end{aligned} \tag{21}$$

where $\varphi_i \in A$ is an occupied spin-orbital of the neutral cluster localized on the subunit A. Note that we are now working with two-hole (2h, $J=1$), three-hole one-particle (3h1p, $J=2$),... excitation classes. Upon diagonalization of the Hamiltonian constructed in the restricted basis of intermediate states generated from the CESs of Eq. (21), the approximation to the initial state is identified as the eigenstate of the desired symmetry with the largest overlap with the 2h configuration describing the initial two vacancies. The approximate continuum components, $\chi_{\beta\varepsilon}$, corresponding to the possible final states of the interatomic decay, are obtained in a separate ADC(n) calculation as the eigenstates of the 3h1p character:

$$\chi_{\beta,\epsilon}\sim\Psi_q^{3h1p} = \sum_i\sum_{|J|=i} Y_{q,J}\tilde{\Psi}_J,\ 1-\sum_{|J|=2}|Y_{q,J}|^2 \ll 1. \tag{22}$$

Once the ADC(n) approximations for the bound and continuum components of the wave function (5) are constructed, one can use the Stieltjes imaging procedure to renormalize the matrix elements computed with the $\mathcal{L}^2$ wave functions, Ψ_q^{3h1p} and interpolate

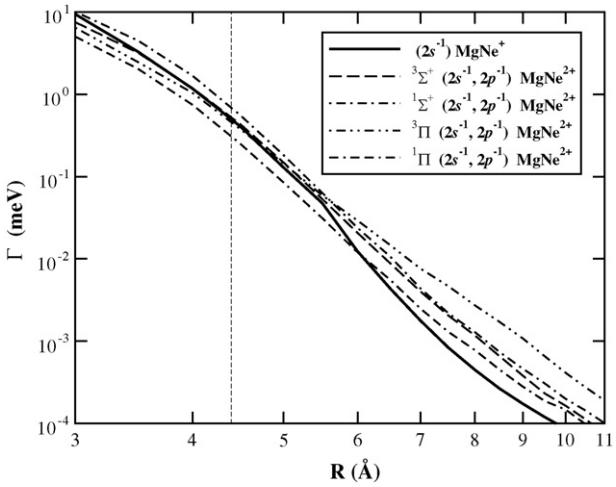

Fig. 7. Doubly logarithmic plot of the total non-radiative decay width of $MgNe^{2+}(2^{s-1}2^{p-1})$ excited state of different spatial symmetries and spin multiplicities. For reference, the full line shows the ICD width of the single Ne 2*s* vacancy. The equilibrium distance of MgNe in the ground state is shown by vertical dashed line.

them in energy as necessary for the computation of the decay widths.

4.3. Auger-ICD cascades in rare gas–alkaline earth clusters

To demonstrate the similarities and differences between ICD in singly and doubly ionized clusters let us investigate the non-radiative decay widths of doubly ionized $(2s^{-1}2p^{-1})$ Ne^{2+} in MgNe diatomic. In the picture provided by the first order of perturbation theory, the decay process proceeds in the same way as ICD of the single Ne 2*s* vacancy, since the initial Ne 2*p* vacancy is only a spectator. Higher orders of perturbation theory involve also pathways in which the initial Ne 2*p* vacancy participates actively, but partial width analysis show that these processes account only for about 5% of the total decay width. The qualitative similarity of the two decay processes is confirmed in Fig. 7, which shows the total non-radiative decay widths of different symmetries of $MgNe^{2+}(2^{s-1}2^{p-1})$ as functions of internuclear distance *R*. The decay width of $MgNe^{+}(2^{s-1})$ is shown as the full line for reference. At large distances all the widths follow the $\Gamma(R) \propto R^{-6}$ law, predicted by the virtual photon model for dipole–dipole interatomic decay processes. At smaller distances around the equilibrium geometry the overlap between atomic orbitals of the two involved atoms leads to significant enhancement of ICD widths as in the case of ICD of singly ionized cluster. Note, however, that the overlap enhancement is less pronounced, in particular in the case of triplet initial states.

It turns out that, although the spectator Ne 2*p* vacancy does not affect significantly the qualitative behavior of the interatomic decay rates, it has very strong impact on the magnitude of the widths. For example, at $R = 12$ Åthe decay width of the $^1\Sigma+$ state of $MgNe^{2+}(2^{s-1}2^{p-1})$ is about 2 times larger than the width of the singly ionized cluster and the width of the $^3\Pi$ state is even 3.5 times larger. The change in the magnitude in the presence of additional vacancy is caused mainly by two factors. First, the electron missing in the 2*p* shell reduces the number of decay pathways, which increases the lifetime of the decaying state. On the other hand, spatial orbitals of multiply ionized atom or molecule are more compact, which increases their Coulombic coupling and in turn also the efficiency of the energy-transfer dominated pathways of the interatomic decay process. The competition of these two effect explains why, at large distances where the energy-transfer character of the decay prevails, the excited doubly ionized states decay faster. In the orbital overlap dominated region, on the other hand, the compactness of the atomic orbitals leads to reduction of the overlap enhancement, in particular for the triplet initial states.

To understand more deeply the diverse magnitudes of the total decay widths of various doubly ionized states of different spatial symmetry and spin multiplicity, particular decay pathways and corresponding partial decay widths have to be analyzed. It appears that, for the $^3\Sigma+$ initial state in particular, the vacancy in the 2*p* shell can impede certain very important decay pathways. For a thorough discussion the reader is referred to Ref. [69].

4.4. Auger-ICD cascade in Ne_2

While Auger-ICD cascades in heteronuclear clusters still await their experimental realization, experiments in homonuclear diatomics provide an interesting bulk of data that has been recently analyzed theoretically. The ICD electron spectra after Auger decay of the 1*s* hole in the Ne dimer was studied in detail in [32]. The time evolutions of the partial ICD spectra were computed by applying the time-dependent theory for the nuclear wave packet dynamics utilizing *ab initio* PECs from [33] shown in Fig. 6. In the calculations [32], an instantaneous Auger decay of the $(1s^{-1})$ Ne_2^+ states has been assumed in the first step of the cascade, since the lifetime of the $K - LL$ Auger decay in the Ne atom is by two orders of magnitude shorter than the typical time for the vibrational motion in the above state (see discussion in Section 4.1). The following model was applied in [32] in order to simulate the ICD transition rates. First, the R^{-6} analytical behavior reflecting the dipole–dipole nature of the interaction governing the ICD at large distances [67,16] was assumed. Second, the absolute value of the total ICD rate was equalized to 8.2 meV as computed in [24] at $R = 3.2$ Å (equivalent to the lifetime of 80 fs). Third, the partial decay rates for all ICD channels were taken to be equal, and each partial decay channel has been assumed energetically closed on the left side of the corresponding curve crossing point.

The total ICD spectrum obtained as the sum of the partial spectra over all possible initial and final ICD states assuming their statistical population via the K-$L_1L_{2,3}$(P1) Auger decay is compared in Fig. 8a with the experimental one [30]. In order to illustrate the impact of the underlying nuclear dynamics, the model spectra obtained as a 'mirror-reflection' of the norm of the initial wave packet $|\Psi_i(\nu = 0)|^2$ on the final repulsive ICD potential energy curve is also shown in Fig. 8a by dashed curve. This model supposes instantaneous ICD transition leaving no time for the nuclear dynamics. Comparing the solid and dashed curves in Fig. 8a, one can see that the nuclear dynamics considerably influences the ICD spectrum. Indeed, the asymmetry in the shape of the total ICD spectrum including the shoulder on its low electron energy side as well as the shift of its maximum to lower energies compared to the vertical electronic transition are due to the nuclear dynamics accompanying the electronic decay.

More recently, the impact of the recoil by the fast Auger electron on the internal nuclear dynamics was observed in [72] by analyzing the partial coincidence ICD spectra following the 1s-ionization of the Ne dimer. The interpretation of the recoil effect is based on the theory given in Ref. [73]. The ICD electron spectrum provides a time averaged 'mirror-reflection' image of the nuclear wave packet propagating on the initial PES onto the final repulsive PES [32]. The energy difference between the initial and the final ICD transition states (the energy of the emitted ICD electron) decreases when going to smaller internuclear distances becoming zero at the corresponding crossing point (see Fig. 6). Obviously, the energy of the emitted ICD electron is closely related to the internuclear geometry at the decay time. During the intra-atomic K-LL Auger decay the fast Auger electron is emitted from the atom where the initially

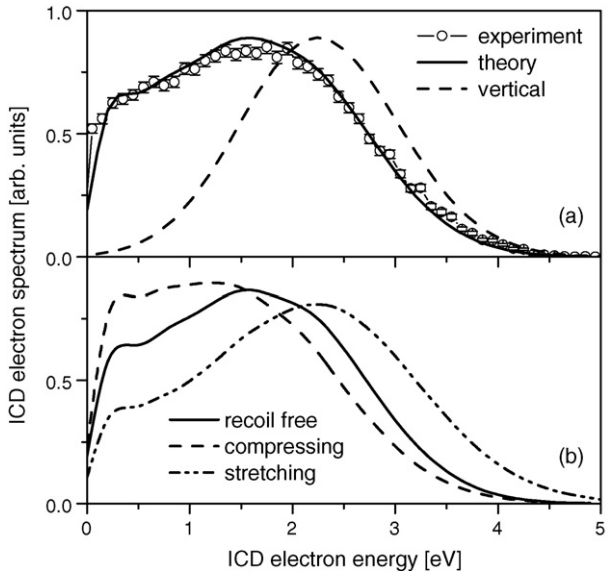

Fig. 8. Total ICD electron spectra for the decay of the $(2s^{-1}2^{p-1}P1)$ $Ne^{2+}Ne$ states into the manifold of the $(2p^{-2}\,{}^1D, 2p^{-1})Ne^{2+}$–$Ne^{+}$ states, after Auger decay of the $(1s^{-1})$ $Ne_2{}^{+}$ state. Panel (a): comparison between the theory [32] and experiment [30]. Panel (b): computational results [73] for different recoil modes induced by the fast Auger electron.

created core-hole was localized, thus, imparting recoil momentum onto this atom which finally becomes Ne^{2+}. After the ICD transition has taken place, the Ne^{+} and Ne^{2+} ions repeal each other strongly, and dissociation along the internuclear axis occurs. If the fast Auger electron is emitted in the direction of the detection of the Ne^{2+} fragment, the recoil momentum is in the direction of Ne^{+} and tends to compress the Ne^{2+}/Ne system. In the opposite case, if the fast Auger electron is emitted in the direction of the detection of the Ne^{+} fragment, the recoil momentum tends to stretch the dimer. The PESs of the $Ne^{2+}Ne$ initial ICD states, which are the final states of the K-LL Auger decay, are very shallow [33] and have a dissociation energy of about 250 meV. The Auger electron kinetic energy loss due to recoil can be estimated as $\Delta E = E_e(m_e/M_{Ne}) \approx 22$ meV. As can be seen in Fig. 8, the ICD processes following the emission of a fast electron provide a sensitive tool to study the recoil effect.

It was illustrated [72,73] that in the compressing mode, the wave packet starts to propagate on the PES of the initial ICD state inwards with an initial velocity provided by the recoil. As a result, the dimer spends more time at smaller internuclear distances, resulting in a preferable emission of the low energy ICD electrons. In the stretching mode, the wave packet starts to propagate outwards with an initial velocity opposite to that in the compressing mode. It turns back and only then moves inwards. As a result, the dimer spends more time at larger internuclear distances, and high energy ICD electrons are preferably emitted. As seen from Fig. 8b taken from Ref. [73], the total ICD spectrum computed for the compressing mode (dashed curve) is considerably enhanced on the low electron energy side, and in the case of the stretching mode (dash-dot-dotted curve) it is enhanced on the high energy side (to be compared with the total ICD spectrum for the vibrational recoil free mode depicted by a solid curve). A notable difference between the ICD spectra measured for the compressing and stretching modes has been unambiguously observed experimentally [72].

5. Outlook

The preceding sections outlined a remarkable activity, both theoretical and experimental, aiming at in-depth study of interatomic decay processes. A manifold of new physical processes have been observed and still more new phenomena have been predicted theoretically. The first demonstration-of-principle experiment has been performed showing the potential of ICD electron spectroscopy as an analytical technique for the study of interfaces [18]. All these developments clearly point at the study of interatomic decay in clusters as at an emerging field of research. Key to theoretical progress in this new field is the ability to obtain reliable estimations of the rates of the various interatomic decay processes. Here, the Fano-ADC approach described in present paper seems to be the method of choice. While established fairly well for singly and doubly ionized systems, the Fano-ADC technique is yet to be generalized to the case of triply ionized states. Furthermore, it would be desirable to extend the existing Fano-ADC approaches for singly ionized states to the ADC(3) and ADC(4) levels of the *ab initio* theory. Indeed, going to the ADC(3) level of approximation of the many-electron states will help to describe the decay of inner-valence-ionized states more accurately than it is done on the currently implemented ADC(2)x level. This could be very important for the vacancy states of elements beyond the second row of periodic table (e.g. $3s^{-1}$ Ar^{+}). ADC(4) level of theory would provide a quantitative description of double decay processes (e.g., DICD) as well as highly accurate results for the decay of core-ionized states. As plausible applications of the envisaged *ab initio* theory, one could cite, for example, the rich pattern of interatomic decay processes in endohedral fullerenes. Of particular interest is the question of the relative time scale of the various single and double decay processes as well as the possible interrelation between ultrafast character of ICD in these systems and the fullerene plasmon.

While the experiment has so far targeted rare gas clusters, a solid theoretical evidence for interatomic decay in other systems, such as hydrogen bonded clusters and endohedral fullerenes, represents an excellent motivation for bringing some chemical diversity into the experimental studies. First steps along this direction have been taken by Hergenhahn and co-workers who have been able to measure ICD in inner-valence-ionized water clusters [74], Dörner, Jahnke and co-workers who performed coincidence measurements on ICD in water dimer [75] and by Aziz et al. who have identified an ICD process involving a 1*s*-ionized OH^{-} ion and a water molecule in NaOH solution [76]. Relevance of interatomic decay processes for water and water solutions naturally leads to the question of the relevance of ICD for biochemical environment, e.g. in the processes leading to radiation damage. At present, this direction is only very little explored and certainly has a high potential for future studies.

A separate chapter in the experimental study of electronic decay has been opened with the advent of new high-frequency radiation sources: attosecond lasers [77] and free electron lasers (FELs) reaching the X-ray regime [78]. Attosecond lasers operating in the XUV domain provide a unique opportunity to study the electronic decay processes in time domain using the so-called streaking probe [79]. The moderate photon energies needed to initiate interatomic decay, together with the characteristic time scales of 1–100 fs make interatomic decay processes natural candidates for the application of the attosecond pump-probe techniques. The first step towards the time-dependent theoretical description of electronic dynamics in the course of interatomic decay has been already taken [80].

While the intensities of the presently available attosecond pulses do not reach strong field regime (the laser field acting on the electrons is much weaker than the one due to atomic or molecular core), FELs are expected to produce unprecedented field strengths of up to tens of atomic units [78]. Even the FEL pulses available today lead to multiple inner-shell ionization of clusters well within the laser pulse (see, e.g. Ref. [81]). It is, thus, tempting

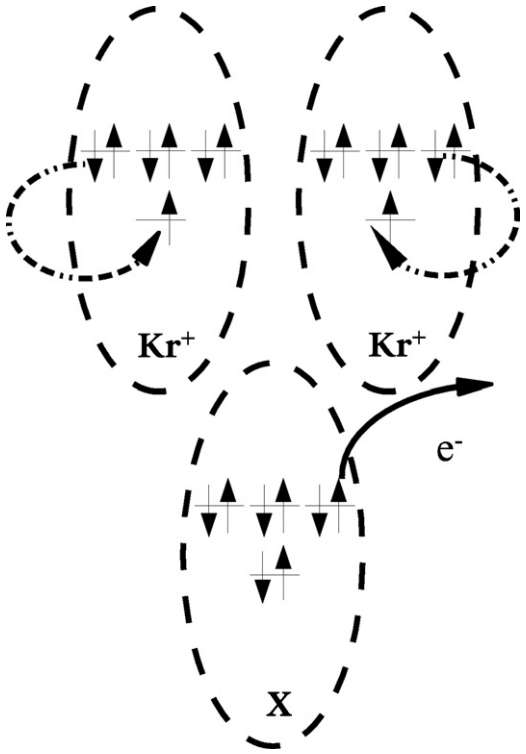

Fig. 9. Schematic representation of collective inter-atomic decay of two inner-shell vacancies: $(4s^{-1}, 4s^{-1})(Kr^+)_2X \rightarrow 2(4p^{-1})Kr^+ + X^+ + e^-$.

to ask whether there are any electronic decay processes that occur exclusively in multiply inner-shell-ionized polyatomic aggregates. A very recent theoretical work [82] shows that such a collective process in which neither of the involved inner-shell vacancies is a spectator, in fact exists. A schematic representation of such a collective decay process that is possible only in a multiply inner-shell-ionized system is given in Fig. 9. It turns out that such the collective decay occurs without facing a competition from the ICD if $1.5 < (E_{iv} - E_c)/E_{ion} < 2$, where E_{iv} is the inner valence ionization energy of the given species, E_c is the energy of Coulombic repulsion between two singly ionized atoms or molecules (typically 3–4 eV at the equilibrium distances of neutral clusters) and E_{ion} is the single ionization energy. Looking at the available ionization energies, one can easily make sure that the collective decay is characteristic of multiple inner-valence-ionized clusters of heavier rare gases (Ar, Kr, Xe), non-metal hydrides having Ar, Kr or Xe as the united atom limit, as well as of clusters of small organic molecules. Study of collective decay in $(4s^{-1}, 4s^{-1})$ $(Kr^+)_2Ar$ [82] suggests that the process is much faster than the radiative decay and can compete successfully with the decomposition of the doubly ionized cluster due to Coulombic explosion. The new collective effect enriches the palette of interatomic decay processes discussed in this review. We suggest to call this type of decay collective ICD (CICD).

In the present paper, we have outlined the major successes and challenges of the study of interatomic decay with the particular emphasis on the development of *ab initio* theoretical methodology. It is our hope that more theoreticians and experimentalists will enter the new fascinating world of interatomic decay and contribute to turning the new basic concepts into a powerful spectroscopic tool.

Acknowledgments

The authors would like to thank Jochen Schirmer for many fruitful discussions in the course of the work described in the present review. V. A. would like to acknowledge financial support of the Max Planck Society through the distinguished PKS postdoctoral fellowship. P. K. acknowledges financial support from the Grant GAČR 202/09/0786 of the Czech Science Foundation. Ph. V. D. would like to acknowledge the European Commission for the Marie Curie fellowship (PIIF-GA-2008-219224). S. S. would like to acknowledge the Japanese Society for the Promotion of Science (JSPS). Financial support of Deutsche Forschungsgemeinschaft is gratefully acknowledged. The research leading to these results has received funding from the European Research Council under the European Community's Seventh Framework Programme (FP7/2007-2013)/ERS Advanced Investigator Grant No. 227597.

References

[1] P. Auger, J. de Phys. 6 (1925) 205.
[2] E.H.S. Burhop, W.N. Asaad, Adv. At. Mol. Phys. 8 (1972) 163;
W. Mehlhorn, in: B. Crasemann (Ed.), Atomic Inner-Shell Physics, Plenum, New York, 1985.
[3] N.H. Turner, J.A. Schreifels, Anal. Chem. 72 (2000) 99R.
[4] C.D. Wagner, A. Joshi, J. Elec. Spectr. Rel. Phen. 47 (1988) 283.
[5] L.S. Cederbaum, J. Zobeley, F. Tarantelli, Phys. Rev. Lett. 79 (1997) 4778.
[6] R. Santra, J. Zobeley, L.S. Cederbaum, N. Moiseyev, Phys. Rev. Lett. 85 (2000) 4490.
[7] M.S. Deleuze, J.-P. Francois, E.S. Kryachko, J. Am. Chem. Soc. 127 (2005) 16824.
[8] S. Marburger, O. Kugeler, U. Hergenhahn, T. Möller, Phys. Rev. Lett. 90 (2003) 203401.
[9] T. Jahnke, A. Czasch, M.S. Schöffler, S. Schössler, A. Knapp, M. Käsz, J. Titze, C. Wimmer, K. Kreidi, R.E. Grisenti, A. Staudte, O. Jagutzki, U. Hergenhahn, H. Schmidt-Böcking, R. Dörner, Phys. Rev. Lett. 93 (2004) 163401.
[10] R. Dörner, V. Mergel, O. Jagutzki, L. Spielberger, J. Ullrich, R. Moshammer, H. Schmidt-Böcking, Phys. Rep. 330 (2000) 95.
[11] S. Scheit, V. Averbukh, H.-D. Meyer, N. Moiseyev, R. Santra, T. Sommerfeld, J. Zobeley, L.S. Cederbaum, J. Chem. Phys. 121 (2004) 8393.
[12] G. Öhrwall, M. Tchaplygine, M. Lundwall, R. Feifel, H. Bergersen, T. Rander, A. Lindblad, J. Schulz, S. Peredkov, S. Barth, S. Marburger, U. Hergenhahn, S. Svensson, O. Björneholm, Phys. Rev. Lett. 93 (2004) 173401.
[13] R. Santra, J. Zobeley, L.S. Cederbaum, Phys. Rev. B 64 (2001) 245104.
[14] N. Vaval, L.S. Cederbaum, J. Chem. Phys. 126 (2007) 164110.
[15] I.B. Müller, L.S. Cederbaum, J. Chem. Phys. 122 (2005) 094305.
[16] V. Averbukh, I.B. Müller, L.S. Cederbaum, Phys. Rev. Lett. 93 (2004) 263002.
[17] V. Averbukh, L.S. Cederbaum, Phys. Rev. Lett. 96 (2006) 053401.
[18] S. Barth, S. Marburger, S. Joshi, V. Ulrich, O. Kugeler, U. Hergenhahn, PCCP 8 (2006) 3218.
[19] S. Barth, S. Joshi, S. Marburger, V. Ulrich, A. Lindblad, G. Öhrwall, O. Björneholm, U. Hergenhahn, J. Chem. Phys. 122 (2005) 241102.
[20] T. Aoto, K. Ito, Y. Hikosaka, F. Penent, P. Lablanquie, Phys. Rev. Lett. 97 (2006) 243401.
[21] W. Eberhardt, G. Kalkoffen, C. Kunz, Phys. Rev. Lett. 41 (1978) 156;
G.C. Brown, M.H. Chen, B. Crasemann, G.E. Ice, Phys. Rev. Lett. 45 (1980).
[22] F. Gel'mukhanov, H. Ågren, Phys. Rep. 312 (1999) 87.
[23] K. Gokhberg, V. Averbukh, L.S. Cederbaum, J. Chem. Phys. 124 (2006) 144315.
[24] R. Santra, L.S. Cederbaum, Phys. Rev. Lett. 90 (2003) 153401.
[25] Y. Morishita, X.-J. Liu, N. Saito, T. Lischke, M. Kato, G. Prümper, M. Oura, H. Yamaoka, Y. Tamenori, I.H. Suzuki, K. Ueda, Phys. Rev. Lett. 96 (2006) 243402.
[26] X.J. Liu, N. Saito, H. Fukuzawa, Y. Morishita, S. Stoychev, A. Kuleff, I.H. Suzuki, Y. Tamenori, R. Richter, G. Prümper, K. Ueda, J. Phys. B: At. Mol. Opt. Phys. F1 (2007).
[27] Y. Morishita, N. Saito, I.H. Suzuki, H. Fukuzawa, X.-J. Liu, K. Sakai, G. Prümper, K. Ueda, H. Iwayama, K. Nagaya, M. Yao, K. Kreidi, M. Schöffler, T. Jahnke, S. Schössler, R. Dörner, T. Weber, J. Harries, Y. Tamenori, J. Phys. B 41 (2008) 025101.
[28] S.D. Stoychev, A.I. Kuleff, F. Tarantelli, L.S. Cederbaum, J. Chem. Phys. 128 (2008) 014307.
[29] K. Kreidi, T. Jahnke, Th. Weber, T. Havermeier, R.E. Grisenti, X. Liu, Y. Morisita, S.L. Schössler, Ph.H. Schmidt, M. Schöffler, M. Odenweller, N. Neumann, L. Foucar, J. Titze, B. Ulrich, F. Sturm, C. Stuck, R. Wallauer, S. Voss, I. Lauter, H.K. Kim, M. Rudloff, H. Fukuzawa, G. Prümper, N. Saito, K. Ueda, A. Czasch, O. Jagutzki, H. Schmidt-Böcking, S.K. Semenov, N.A. Cherepkov, R. Dörner, J. Phys. B 41 (2008) 101002.
[30] K. Kreidi, T. Jahnke, Th. Weber, T. Havermeier, X. Liu, Y. Morisita, S.L. Schössler, Ph.H. Schmidt, M. Schöffler, M. Odenweller, N. Neumann, L. Foucar, J. Titze, B. Ulrich, F. Sturm, C. Stuck, R. Wallauer, S. Voss, I. Lauter, H.K. Kim, M. Rudloff, H. Fukuzawa, G. Prümper, N. Saito, K. Ueda, A. Czasch, O. Jagutzki, H. Schmidt-Böcking, S. Stoychev, Ph.V. Demekhin, R. Dörner, Phys. Rev. A 78 (2008) 043422.
[31] M. Yamazaki, J. Adachi, Y. Kimura, A. Yagishita, M. Stener, P. Decleva, N. Kosugi, H. Iwayama, K. Nagaya, M. Yao, Phys. Rev. Lett. 101 (2008) 043004.
[32] Ph.V. Demekhin, S. Scheit, D. Stoychev, L.S. Cederbaum, Phys. Rev. A 78 (2008) 043421.
[33] S.D. Stoychev, A.I. Kuleff, F. Tarantelli, L.S. Cederbaum, J. Chem. Phys. 129 (2008) 074307.

[34] Ph.V. Demekhin, Y.C. Chiang, S.D. Stoychev, P. Kolorenč, S. Scheit, A.I. Kuleff, F. Tarantelli, L.S. Cederbaum, J. Chem. Phys. 131 (2009) 104303.
[35] K. Ueda, private communication.
[36] L.S. Cederbaum, F. Tarantelli, J. Chem. Phys. 98 (1993) 9691.
[37] S. Scheit, L.S. Cederbaum, H.-D. Meyer, J. Chem. Phys. 118 (2003) 2092.
[38] S. Scheit, V. Averbukh, H.-D. Meyer, J. Zobeley, L.S. Cederbaum, J. Chem. Phys. 124 (2006) 154305.
[39] N. Moiseyev, R. Santra, J. Zobeley, L.S. Cederbaum, J. Chem. Phys. 114 (2001) 7351.
[40] F.K. Gel'mukhanov, L.N. Mazalov, A.V. Kondratenko, Chem. Phys. Lett. 46 (1977) 133.
[41] S. Scheit, L.S. Cederbaum, Phys. Rev. Lett. 96 (2006) 233001.
[42] N. Moiseyev, Phys. Rep. 302 (1998) 211.
[43] N. Moiseyev, S. Scheit, L.S. Cederbaum, J. Chem. Phys. 121 (2004) 722.
[44] U.V. Riss, H.D. Meyer, J. Phys. B 26 (1993) 4593.
[45] J.G. Muga, J.P. Palao, B. Navarro, I.L. Egusquiza, Phys. Rep. 395 (2004) 357.
[46] R. Santra, L.S. Cederbaum, H.-D. Meyer, Chem. Phys. Lett. 303 (1999) 413.
[47] N. Moiseyev, J. Phys. B 31 (1998) 1431;
U.V. Riss, H.-D. Meyer, J. Phys. B 31 (1998) 2279.
[48] J. Schirmer, L.S. Cederbaum, O. Walter, Phys. Rev. A 28 (1983) 1237;
L.S. Cederbaum, in: P.V.R. Schleyer, P.R. Schreiner, N.A. Allinger, T. Clark, J. Gasteiger, P. Kollman, H.F. Schaefer III (Eds.), Encyclopedia of Computational Chemistry, Wiley, New York, 1998.
[49] R. Santra, L.S. Cederbaum, Phys. Rep. 368 (2002) 1.
[50] A.B. Trofimov, J. Schirmer, J. Chem. Phys. 123 (2005) 144115.
[51] I.B. Müller, Ph.D. thesis, Universität Heidelberg, 2006, in German.
[52] H. Hennig, Diploma thesis, Universität Heidelberg, 2004, in German.
[53] V. Averbukh, L.S. Cederbaum, J. Chem. Phys. 123 (2005) 204107.
[54] U. Fano, Phys. Rev. 124 (1961) 1866.
[55] J. Schirmer, Phys. Rev. A 43 (1991) 4647;
F. Mertins, J. Schirmer, Phys. Rev. A 53 (1996) 2140;
A.B. Trofimov, J. Schirmer, J. Chem. Phys. 123 (2005) 144115.
[56] P.W. Langhoff, in: T. Rescigno, V. McKoy, B. Schneider (Eds.), Electron-Molecule and Photon-Molecule Collisions, Plenum, New York, 1979; A.U. Hazi, in: T. Rescigno, V. McKoy, B. Schneider (Eds.), Electron-Molecule and Photon-Molecule Collisions, Plenum, New York, 1979.
[57] G. Howat, T. Åberg, O. Goscinski, J. Phys. B 11 (1978) 1575.
[58] T. Åberg, G. Howat, in: W. Mehlhorn (Ed.), Handbuch der Physik, vol. 31, Springer, Berlin, 1982.
[59] A. Szabo, A.S. Ostlund, Modern Quantum Chemistry: Introduction to Advanced Electronic Structure Theory, Dover, New York, 1996.
[60] J. Schirmer, A.B. Trofimov, G. Stelter, J. Chem. Phys. 109 (1998) 4734.
[61] E. Davidson, J. Comp. Phys. 17 (1975) 87.
[62] V. Averbukh, L.S. Cederbaum, J. Chem. Phys. 125 (2006) 094107.
[63] F. Müller-Plathe, G.H.F. Diercksen, in: S. Canuto, J. D'Albuquerque e Castro, F.J. Paixã o (Eds.), Electronic Structure of Atoms, Molecules and Solids, World Scientific, Singapore, 1990; F. Müller-Plathe, G.H.F. Diercksen, Phys. Rev. A 40 (1989) 696.
[64] J.A.D. Matthew, Y. Komninos, Surf. Sci. 63 (1975) 716.
[65] T.D. Thomas, C. Miron, K. Wiesner, P. Morin, T.X. Carroll, L.J. Sæthre, Phys. Rev. Lett. 89 (2002) 223001.
[66] D.C. Griffin, D.M. Mitnick, N.R. Randell, J. Phys. B 34 (2001) 4401.
[67] R. Santra, L.S. Cederbaum, J. Chem. Phys. 115 (2001) 6853.
[68] T. A. Carlson, M.O. Krause, Phys. Rev. Lett. 14 (1965) 390; Phys. Rev. Lett. 17 (1966) 1079.
[69] P. Kolorenč, V. Averbukh, K. Gokhberg, L.S. Cederbaum, J. Chem. Phys. 129 (2008) 244102.
[70] S. Scheit, PhD thesis, Ruprecht-Karls-Universität Heidelberg, 2007.
[71] J. Schirmer, A. Barth, Z. Phys. A 317 (1984) 267.
[72] K. Kreidi, Ph.V. Demekhin, T. Jahnke, T. Weber, T. Havermeier, X. Liu, Y.M.S. Schössler, L.P.H. Schmidt, M. Schöffler, M. Odenweller, N. Neumann, L. Foucar, J. Titze, B. Ulrich, F. Sturm, C. Stuck, R. Wallauer, S. Voss, I. Lauter, H.K. Kim, M. Rudloff, H. Fukuzawa, G. Prümper, N. Saito, K. Ueda, A. Czasch, O. Jagutzki, H. Schmidt-Böcking, S. Scheit, L.S. Cederbaum, R. Dörner, Phys. Rev. Lett. 103 (2009) 033001.
[73] Ph.V. Demekhin, S. Scheit, L.S. Cederbaum, J. Chem. Phys. 131 (2009) 164301.
[74] M. Mucke, M. Braune, S. Barth, M. Förstel, T. Lischke, V. Ulrich, T. Arion, A.M. Bradshaw, U. Becker, U. Hergenhahn, Nat. Phys 6 (2010) 143.
[75] T. Jahnke, H. Sann, T. Havermeier, K. Kreidi, C. Stuck, M. Meckel, M. Schöffler, N. Neumann, R. Wallauer, S. Voss, A. Czasch, O. Jagutzki, A. Malakzadeh, F. Afaneh, T. Weber, H. Schmidt-Böcking, R. Dörner, Nat. Phys 6 (2010) 139.
[76] E.F. Aziz, N. Ottoson, M. Faubel, I.V. Hertel, B. Winter, Nature 455 (2008) 89.
[77] M. Hentschel, R. Kienberger, Ch. Spielmann, G.A. Reider, N. Milosevic, T. Brabec, P. Corkum, U. Heinzmann, M. Drescher, F. Krausz, Nature 414 (2001) 509;
G. Sansone, E. Benedetti, F. Calegari, C. Vozzi, L. Avaldi, R. Flammini, L. Poletto, P. Villoresi, C. Altucci, R. Velotta, S. Stagira, S. De Silvestri, M. Nisoli, Science 314 (2006) 443.
[78] M.A. Kornberg, A.L. Godunov, S. Itza-Ortiz, D.L. Ederer, J.H. McGuire, L. Young, J. Synchrotron Rad. 9 (2002) 298, See e.g.
[79] M. Drescher, M. Hentschel, R. Kienberger, M. Uiberacker, V. Yakovlev, A. Scrinzi, Th. Westerwalbesloh, U. Kleineberg, U. Heinzmann, F. Krausz, Nature 419 (2002) 803.
[80] A.I. Kuleff, L.S. Cederbaum, Phys. Rev. Lett. 98 (2007) 083201.
[81] U. Saalmann, J.M. Rost, Phys. Rev. Lett. 89 (2002) 143401.
[82] V. Averbukh, P. Kolorenč, Phys. Rev. Lett. 103 (2009) 183001.